Journal of Solid State Chemistry 182 (2009) 2867–2872

Contents lists available at ScienceDirect

Journal of Solid State Chemistry

journal homepage: www.elsevier.com/locate/jssc

Utilization of iron oxide film obtained by CVD process as catalyst to carbon nanotubes growth

Mariane C. Schnitzler, Aldo J.G. Zarbin *

Departamento de Química, Universidade Federal do Paraná, CP 19081, CEP 81531-990, Curitiba, PR, Brazil

ARTICLE INFO

Article history:
Received 12 May 2009
Received in revised form
28 July 2009
Accepted 30 July 2009
Available online 6 August 2009

Keywords:
Iron oxide film
Carbon nanotubes
Chemical vapor deposition

ABSTRACT

Thin films of Fe_2O_3 were obtained on silica glass substrates through the thermal decomposition of ferrocene in air. These films were characterized by Raman spectroscopy and X-ray diffractometry (XRD), and subsequently used as catalyst on the growth of carbon nanotubes, using benzene or a benzene solution of $[Fe_3(CO)_{12}]$ as precursor. A great amount of a black powder was obtained as product, identified as multi-walled carbon nanotubes by XRD, Raman spectroscopy and transmission electron microscopy. The carbon nanotubes formed through the pyrolysis of the $[Fe_3(CO)_{12}]$ solution were identified as structurally better than the one obtained by the pyrolysis of pristine benzene.

1. Introduction

Since their first report in 1991 [1], carbon nanotubes (CNTs) have attracted great interest of the scientific community, due to their unprecedented properties. Carbon nanotubes can be prepared through several methods, as arc-discharge [1], laser ablation [2], or chemical vapor deposition (CVD). The CVD process has been one of the most explored routes to prepare CNTs. This method is based on the thermal decomposition of a carbon precursor under a controlled atmosphere and temperature in the presence of a catalyst. The most used carbon precursors are hydrocarbon compounds as acetylene, methane, benzene and ethylene; and the catalyst is usually based on metal nanoparticles as Fe, Ni and Co [3–5]. Our research group has been working on the utilization of organometallic compounds as precursors for CNT by CVD [6], spray pyrolysis [7] or solid-state [8] processes. Although the most used catalysts to CNT growing are metal nanoparticles, some transition metal oxides have also been successfully employed. For example, Kim et al. [9] have obtained ultra-long semiconducting single-walled CNTs using Fe_2O_3 nanoparticles as catalyst, and a mixture of methane/ethylene/hydrogen as carbon source. Rummeli and co-workers [10] have demonstrated the high efficiency on the utilization of several metal oxides (as Fe_2O_3, In_2O_3, MgO and PbO_2) as catalysts in the CNT synthesis by the laser ablation route. Fu et al. [11] have studied the CVD-growth single-walled carbon nanotubes employing Fe_2O_3 nanoclusters prepared in inverse micelles as catalyst. Dai and Skourtis [12] reported the preparation of self-aligned CNT forest using FeO as catalyst. Barreca et al. have obtained multi-walled carbon nanotubes using mesoporous silica impregnated with iron oxide nanoparticles as catalyst [13]. A very interesting paper related to the use of iron oxide as catalyst to CNTs has been recently published by Sato and co-workers [14]. These authors concluded that the Fe_2O_3 itself does not have catalytic activity, but the Fe_2O_3 nanoparticles are reduced to metallic iron during the CNTs growth process.

In this work we present a novel approach of preparing a thin film of Fe_2O_3 over a flat silica glass substrate, and the subsequent utilization of this film as catalyst on the synthesis of carbon nanotubes.

2. Experimental

2.1. Chemicals

Acetone (Merck), benzene (Merck), iron dodecacarbonyl (Merck) and hydrochloridic acid (Merck) were used as received. Ferrocene (Fluka) was purified by sublimation before use. Water was distilled and Milli-Q deionized before use. The porous Vycor glass (PVG) plates (Corning 7930) were cut in $10 \times 10 \times 1$ mm, and treated in order to remove impurities adsorbed on their pores. The plates were immersed in a 2 mol L^{-1} HCl solution for 30 min, washed with deionized water, dried, immersed in acetone for 30 min, dried, left at 550 °C for 72 h, cooled to room temperature and stored in a desiccator prior to use.

* Corresponding author. Fax: +55 41 33613186.
E-mail address: aldo@quimica.ufpr.br (A.J. Zarbin).

0022-4596/$ - see front matter © 2009 Elsevier Inc. All rights reserved.
doi:10.1016/j.jssc.2009.07.057

2.2. Synthesis of Fe_2O_3 films

A quartz tube (36 mm diameter and 750 mm length) was placed in a two-stage furnace system, and air was continuously passed through the tube employing an air compressor (flow rate 300 mL min^{-1}). A known quantity (0.5 g) of purified ferrocene (Fluka) was taken in a quartz boat and placed inside the first furnace. The ferrocene was sublimed by raising the temperature of this furnace to 300 °C at a heating rate of 40 °C min^{-1}. The vapor was carried by the air flow into the second furnace kept at 900 °C, in which a piece of a porous Vycor glass ($10 \times 10 \times 1$ mm) was previously added. After 2 h of the beginning of sublimation the furnace system was turned off. A red, transparent and homogeneous film was obtained on the PVG substrate surface and on the quartz tube walls.

2.3. Synthesis of carbon nanotubes using benzene as precursor

A quartz tube (36 mm diameter and 750 mm length) was placed in a furnace system, and an argon flux was passed through the tube during 30 min at room temperature, before the beginning of heating. The substrates (both PVG plate and PVG plate containing the iron oxide film on its surface prepared according described earlier) were previously loaded in the medium zone of the tubular furnace. A gas-scrubber containing benzene (35 mL) was connected to the entrance of the quartz tube. The furnace system was heated under argon flow until 900 °C, and when this temperature was reached, an argon flow was continuously passed through the benzene-containing gas-scrubber, producing benzene vapors which were arrested by the argon flux to the hot zone of the quartz tube. After 30 min, the system was turned off and cooled under argon atmosphere down to room temperature. A black solid powder was formed on the substrates surface and on the quartz tube walls.

2.4. Synthesis of carbon nanotubes using $[Fe_3(CO)_{12}]$/benzene solution as precursor

The synthesis of CNTs starting from the $[Fe_3(CO)_{12}]$ solution in benzene was based on the spray pyrolysis route, employing the apparatus described in detail in Ref. [7]. In summary, a saturated benzene solution of $[Fe_3(CO)_{12}]$ (20 mL, saturated solution is approximately 0.5 wt%) was freshly prepared and put in an aerosol generator connected to the apparatus in which the pyrolysis took place. A quartz tube (36 mm diameter and 750 mm length) was placed in a tubular furnace and argon was passed to the tube. The substrates (both PVG plate and PVG plate containing the iron oxide film on its surface prepared according described earlier, size $10 \times 10 \times 1$ mm) were previously loaded in the medium zone of the tubular furnace. The furnace temperature was raised up to 900 °C, and subsequently the argon flow was passed through the $[Fe_3(CO)_{12}]$ solution, creating the aerosol that was carried to the furnace. The glass aerosol generator apparatus consists of a reservoir and two concentric tubes in which one of the tubes is in contact with the $[Fe_3(CO)_{12}]$ solution (see Ref. [7] for details). When this system is submitted to a high argon flow, a pressure difference is created drawing the solution through the orifice of the inner tube, originating aerosol which is carried to the interior of the pyrolysis system. After 30 min the aerosol generation was discontinued and the furnace system was turned off. The furnace was allowed to cool to room temperature under argon flow. The pyrolysis yielded large amounts of carbon deposited on the substrates surface and on the quartz tube wall.

2.5. Physical characterization

The X-ray diffraction (XRD) patterns were collected in a Shimadzu XRD-6000 diffractometer with Cu$K\alpha$ radiation at 40 kV and 40 mA. The substrates in which the samples were obtained were put directly on the sample compartment of the equipment, and the diffractograms were directly collected from the as-growth samples at a rate of 2° min^{-1} (in 2θ), using silicon powder as a reference.

The Raman spectra were obtained in a Renishaw Raman-image spectrophotometer coupled to an optical microscope that focuses the incident radiation down to an approximately 1 μm spot. An argon laser ($\lambda = 514.5$ nm) was used with 2 mW incidence potency over the 180–3000 cm^{-1} region. The spectra were collected on the as-growth samples, as deposited on the substrate surface.

The transmission electron microscopy (TEM) analyses were performed in a Jeol (JEM 1200 EXII, 120 KeV) microscope. The samples were scratched from the substrate and dispersed in *N*,*N*-dimethylformamide (DMF). A drop of the supernatant dispersion was placed onto a carbon film supported by a copper grid.

3. Results and discussion

This work aims the development of a novel approach to the production of thin film of iron oxide, and its subsequent utilization as catalyst to CNT growth. The iron oxide synthesis was based on the following chemical reaction:

$$4[Fe(C_5H_5)_2](g)+53O_2(g) \rightarrow 2Fe_2O_3(s)+40CO_2(g)+20H_2O(g) \quad (1)$$

Porous Vycor glass (PVG) plates were used as substrates. This is a transparent porous material composed essentially of silica. PVG has interconnecting pores of size distribution between 2 and 20 nm, with a pore volume of nearly 28% [8]. PVG has high thermal stability and its structure can be consolidated at 1200 °C. In this temperature the pores collapse to form a dense, high-silica content glass. The utilization of PVG as substrate here was based on our previous work showing that PVG is very useful substrate to CNTs growth both by CVD and by spray pyrolysis route [6,7].

A red-orange, transparent, homogeneous and adherent film was formed on the PVG substrate surface after the thermal treatment of ferrocene vapors in air. This film was characterized by both Raman spectroscopy and XRD, and was identified as iron oxide. The Raman spectrum of this film is shown in Fig. 1. All

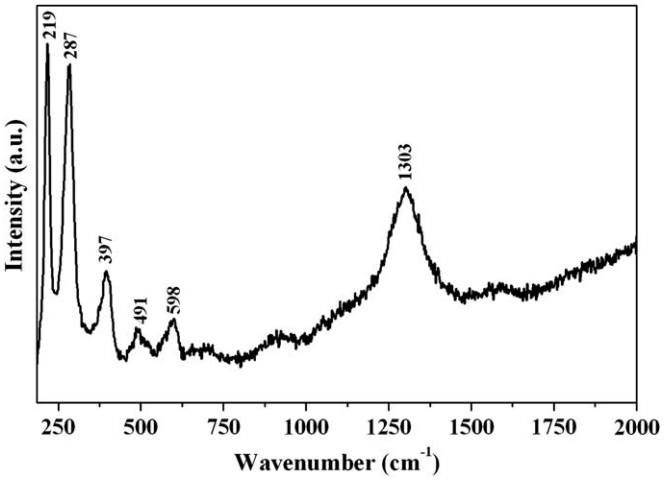

Fig. 1. Raman spectrum of the red film obtained on the PVG surface.

bands are characteristic of α-Fe_2O_3 (hematite) with the following attributions [15]: the bands at 219 and 491 cm^{-1} are due to A_{1g} modes; the bands at 288, 397 and 597 cm^{-1} are related to the E_g modes and the band at 1303 cm^{-1} is an overtone of a forbidden band that should appear in approximately 663 cm^{-1}.

Fig. 2 shows the XRD patterns of the obtained film (Fig. 2b) and of a commercial α-Fe_2O_3 sample (Fig. 2a). In comparison with the commercial sample, it is clear that the film is mainly composed of α-Fe_2O_3, corroborating the data obtained by Raman spectroscopy. It is noticeable, however, the occurrence of three peaks that do not match with peaks due to α-Fe_2O_3 (at $d = 0.926$; 0.713 and 0.623 nm, marked with asterisks in Fig. 2b). Unfortunately we were not able to make a correct attribution to these peaks. A clear amorphous halo can also be seen in the XRD pattern of the film (Fig. 2b), due to glass substrate. The broad peaks present on the XRD pattern of the film indicate short crystallite diameter of the former oxide.

The iron oxide film obtained according to the earlier description was used as catalyst to the CNT growth, starting from either pristine benzene or a benzene solution of [$Fe_3(CO)_{12}$] as precursor. In order to understand the role of the oxide film catalyst on the CNTs growth, a PVG substrate without the oxide film on its surface was also employed as substrate in each synthesis. The product of all pyrolysis was a black material deposited over the substrates. The carbonaceous materials will be referred here as C/benzene/oxide and C/benzene/PVG to the samples obtained from the pyrolysis of pristine benzene on the iron oxide film and pristine PVG substrate, respectively. In the same way, samples C/[$Fe_3(CO)_{12}$]/oxide and C/[$Fe_3(CO)_{12}$]/PVG correspond to the carbonaceous materials resulting from the pyrolysis of the [$Fe_3(CO)_{12}$] solution over the iron oxide film and pristine PVG substrate, respectively.

The importance of the iron oxide film on the resulting carbonaceous materials was initially highlighted by XRD, Fig. 3. The XRD patterns of the samples growth on the pristine PVG substrate (Figs. 3a and b to the samples C/benzene/PVG and C/[$Fe_3(CO)_{12}$]/PVG, respectively) are characteristic of amorphous carbon, with no diffraction peak observable (although a non-attributed signal at $d = 0.773$ nm can be identified in the XRD pattern of the sample C/[$Fe_3(CO)_{12}$]/PVG, Fig. 3b).

Diffraction patterns of both C/benzene/oxide and C/[$Fe_3(CO)_{12}$]/oxide samples (Figs. 3c and d, respectively) show a very different profile, characterized by a graphitic-like peak at $d = 0.34$ nm (marked with an asterisk in Fig. 3), attributed to the distance between the (002) planes in graphitic structures. The d_{002} observed in both XRD patterns are slightly higher than the observed in graphite ($d_{002} = 0.335$ nm), and can be attributed to the curvature of the rolled graphene sheets on the multi-walled carbon nanotubes (MWCNTs) structure [16]. This result should be an indicative of the occurrence of MWCNTs in the C/benzene/oxide and C/[$Fe_3(CO)_{12}$]/oxide samples.

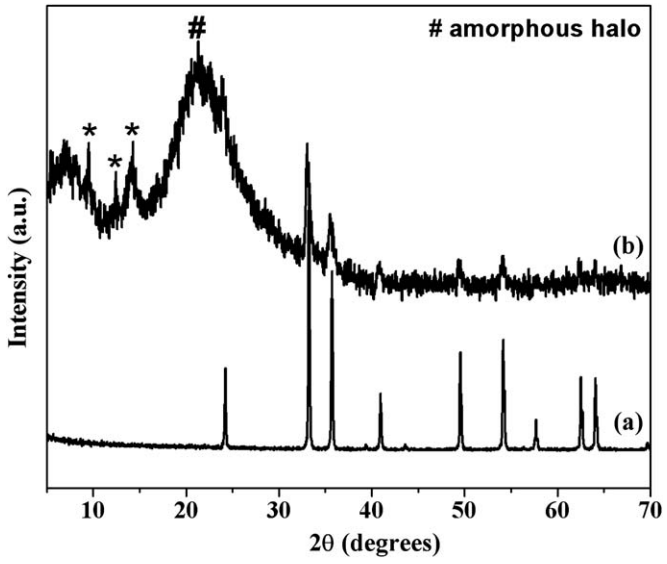

Fig. 2. X-ray diffraction profiles: (a) commercial sample of α-Fe_2O_3 and (b) red film obtained on the PVG surface.

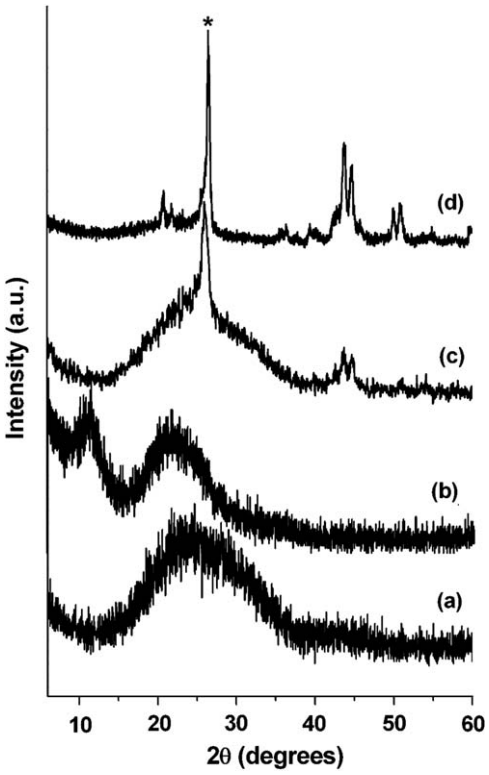

Fig. 3. X-ray diffraction profiles of the carbonaceous samples: (a) C/benzene/PVG; (b) C/[$Fe_3(CO)_{12}$]/PVG; (c) C/benzene/oxide and (d) C/[$Fe_3(CO)_{12}$]/oxide.

Besides the graphite-like peak discussed above, the XRD patterns of both C/benzene/oxide and C/[$Fe_3(CO)_{12}$]/oxide samples show an amorphous halo due to the glass substrate, below the (002) peak. This halo is more intense in the XRD pattern of the C/benzene/oxide sample, which can indicate some other contribution besides the glass substrate (for example due to some fraction of amorphous carbon occasionally present in the sample). Also, it is noticeable that the (002) peak due to MWCNT is much more intense and sharp in the XRD pattern of the sample C/[$Fe_3(CO)_{12}$]/oxide (Fig. 3d) than the C/benzene/oxide (Fig. 3c). This observation can be an indicative that the graphitic structure of the species formed in the C/[$Fe_3(CO)_{12}$]/oxide sample is more organized (contain less defect) than the similar one present in the C/benzene/oxide sample.

Other non-graphitic peaks are clearly observable in both C/[$Fe_3(CO)_{12}$]/oxide and C/benzene/oxide XRD patterns. In the C/benzene/oxide sample (Fig. 3c) all the peaks were attributed to Fe_3C (JCPDF files no. 85-1317). Once there was no iron-containing species in the precursor to this sample (pristine benzene), the Fe_3C formation should be attributed to a reaction between the growing carbonaceous material and the iron oxide of the catalyst film. The occurrence of Fe_3C has been detected in many papers regarding the iron-based catalytic growth of CNTs [6,7,17]. It is interesting that no peaks due the film catalyst were detected in this sample, probably due the thick size of the carbonaceous material that was formed over the substrate. The XRD pattern of

the C/[$Fe_3(CO)_{12}$]/oxide sample (Fig. 3d) also presents Fe_3C peaks, although some low-intensity peaks attributed to α-Fe_2O_3 should be noted. The increase in the intensity of these peaks on the C/[$Fe_3(CO)_{12}$]/oxide sample shows the occurrence of a contribution from the [$Fe_3(CO)_{12}$] present in the precursor solution.

The Raman spectra of the carbonaceous samples are shown in Fig. 4. Two main Raman modes are observable in all the spectra in Fig. 4, at approximately 1590 and 1350 cm^{-1}. The band at about 1590 cm^{-1} is the so-called *G* band, attributed to E_{2g} mode of graphite and related to the vibration of sp^2 carbon atoms in a hexagonal network in two dimensions [18]. The band at about 1350 cm^{-1} is the so-called *D* band, attributed to an in-plane mode which becomes active by small imperfections due to particle size effect and the loss of translational symmetry in the disordered structure [19]. Both the *D* and *G* bands are commonly present in various sp^2 carbonaceous materials, and the frequency, strength and line-width of these bands is found to be a function of the degree of structural disorder of the carbonaceous material [20]. The width and relative intensities of both *G* and *D* lines (I_D/I_G ratio) vary with the ordering of the structure and may be used to characterize carbonaceous materials (a high I_D/I_G ratio can be correlated with a high disorder in the graphitic structure). Shifts to lower frequency, as well as a decrease in the *D* band intensity, are frequently associated to an increase on the degrees of graphitization of the carbonaceous material.

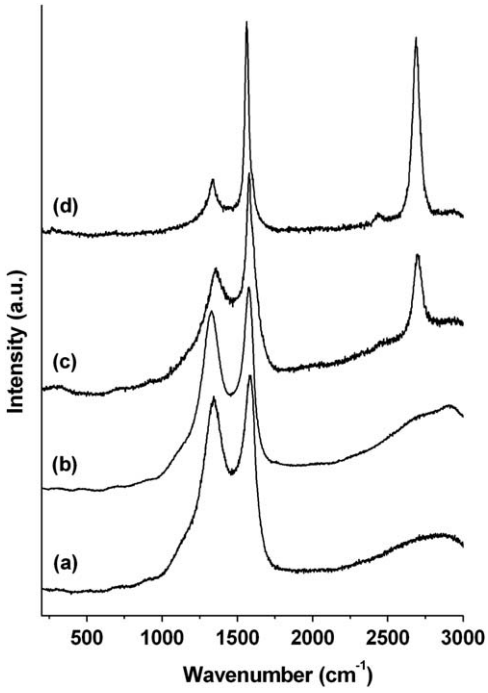

Fig. 4. Raman spectra of the carbonaceous samples: (a) C/benzene/PVG; (b) C/[$Fe_3(CO)_{12}$]/PVG; (c) C/benzene/oxide and (d) C/[$Fe_3(CO)_{12}$]/oxide.

The spectra of the samples obtained over the pristine PVG substrates (C/benzene/PVG and C/[$Fe_3(CO)_{12}$]/PVG, Figs. 4a and b, respectively) present only the *G* and *D* bands, at 1593 and 1353 cm^{-1}, respectively. The *D* bands of both these spectra are broader and intense ($I_D/I_G = 2.20$ and 2.08 for the C/benzene/PVG and C/[$Fe_3(CO)_{12}$]/PVG spectra, respectively), and the spectra profiles are typical of disordered sp^2 carbon material, corroborating the data obtained by XRD.

The carbonaceous materials formed in the C/benzene/oxide and C/[$Fe_3(CO)_{12}$]/oxide samples, however, present different structures, as observable on the Raman spectra present on Figs. 4c and d. These spectra present a shift on the *G* band, when compared with the product formed at samples growth on the pristine PVG substrates. The position of the *G* band was at 1584, 1578, 1574 and 1560 cm^{-1} for the samples C/benzene/PVG, C/[$Fe_3(CO)_{12}$]/PVG, C/benzene/oxide and C/[$Fe_3(CO)_{12}$]/oxide, respectively. As described before, these shifts are associated with an increase in the graphitization degree of the material. This interpretation is corroborated by the appearance of a well-defined band at 2683 cm^{-1} on both the spectra of the carbonaceous materials obtained over the oxide catalyst. This second-order Raman mode is an overtone of the *D* band (this band is usually refereed as *G′* band), and is characteristic of well-graphitized carbon samples, as HOPG and single- or multi-walled carbon nanotubes [21].

The I_D/I_G values obtained for the samples C/benzene/oxide and C/[$Fe_3(CO)_{12}$]/oxide were 1.28 and 0.70, respectively, showing that these samples are more graphitized than the samples obtained without the oxide catalyst. Comparing these two samples, the C/[$Fe_3(CO)_{12}$]/oxide has the lower I_D/I_G ratio, which indicates that this sample is more graphitized than the C/benzene/oxide, corroborating again the data obtained by XRD. The high intensity of the *G′* band in this last sample is another evidence for its better structural quality.

The conclusions obtained from the XRD and Raman data discussed before were corroborated by transmission electron microscopy (TEM). Figs. 5a and b show the TEM images of the samples C/benzene/PVG and C/[$Fe_3(CO)_{12}$]/PVG, respectively.

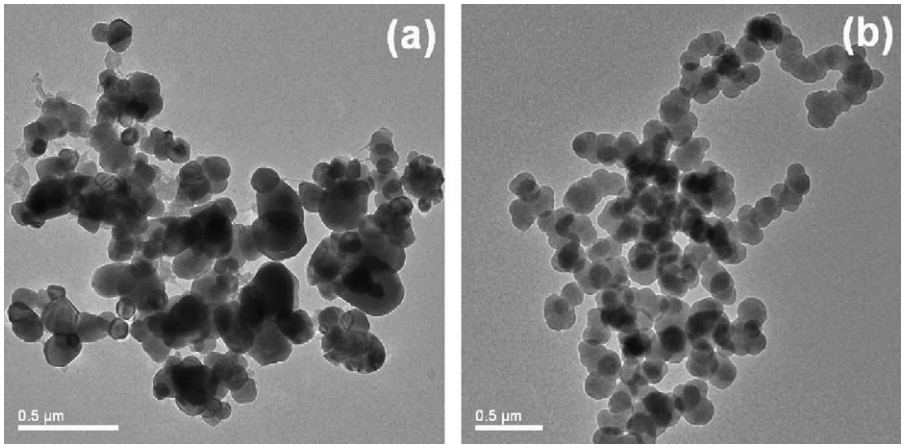

Fig. 5. Transmission electron microscopy images of the carbonaceous samples obtained over the neat PVG substrate: (a) C/benzene/PVG and (b) C/[$Fe_3(CO)_{12}$]/PVG.

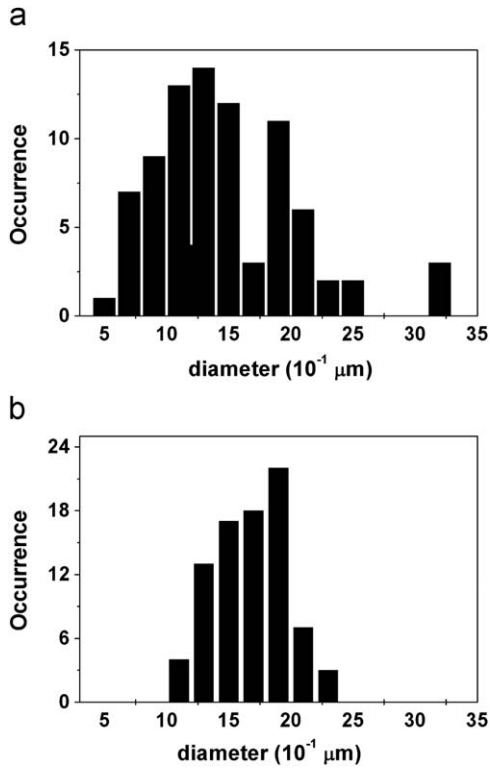

Fig. 6. Size histograms showing the particle diameters distributions of the samples C/benzene/PVG (a) and C/[$Fe_3(CO)_{12}$]/PVG (b).

No carbon nanotubes were detected in these samples. It is clear in both samples the occurrence of agglomerates of carbonaceous material, typical of amorphous carbon. A more detailed analysis of these images presented indicates that the sample C/[$Fe_3(CO)_{12}$]/PVG occurs as more-organized spheres-like particles and with a more homogeneous size distribution, in comparison with the C/benzene/PVG sample, according to the size histograms presented in Fig. 6. The difference between these two samples is also macroscopically detected: the C/benzene/PVG is formed as a fine black powder deposited over the PVG substrate, while the C/[$Fe_3(CO)_{12}$]/PVG is formed as a homogeneous mirror-like film with strong adherence to the PVG substrate. These observations should indicate that, although the [$Fe_3(CO)_{12}$] in benzene solution did not act as catalyst to CNT growth, it has some role in the morphological organization of the carbonaceous material produced.

Fig. 7 shows the TEM images of the samples C/benzene/oxide and C/[$Fe_3(CO)_{12}$]/oxide, confirming the formation of multi-walled carbon nanotubes on both these samples. The sample C/benzene/oxide (Figs. 7a and b) is formed by a large amount of MWNT, containing many imperfections. The nanotubes are long (10–15 μm) and have large diameter distribution (50–250 nm). In contrast, the sample C/[$Fe_3(CO)_{12}$]/oxide is formed basically by bundles of very long and aligned multi-walled carbon nanotubes, showing small defects or imperfection. The images presented in Fig. 7 make clear the important role of the [$Fe_3(CO)_{12}$] on the production of aligned and homogeneous multi-walled carbon nanotube samples. Some nanotubes presented in Figs. 7c and d present their cavities filled with a high-contrast material, probably the iron oxide or iron carbide detected previously by XRD.

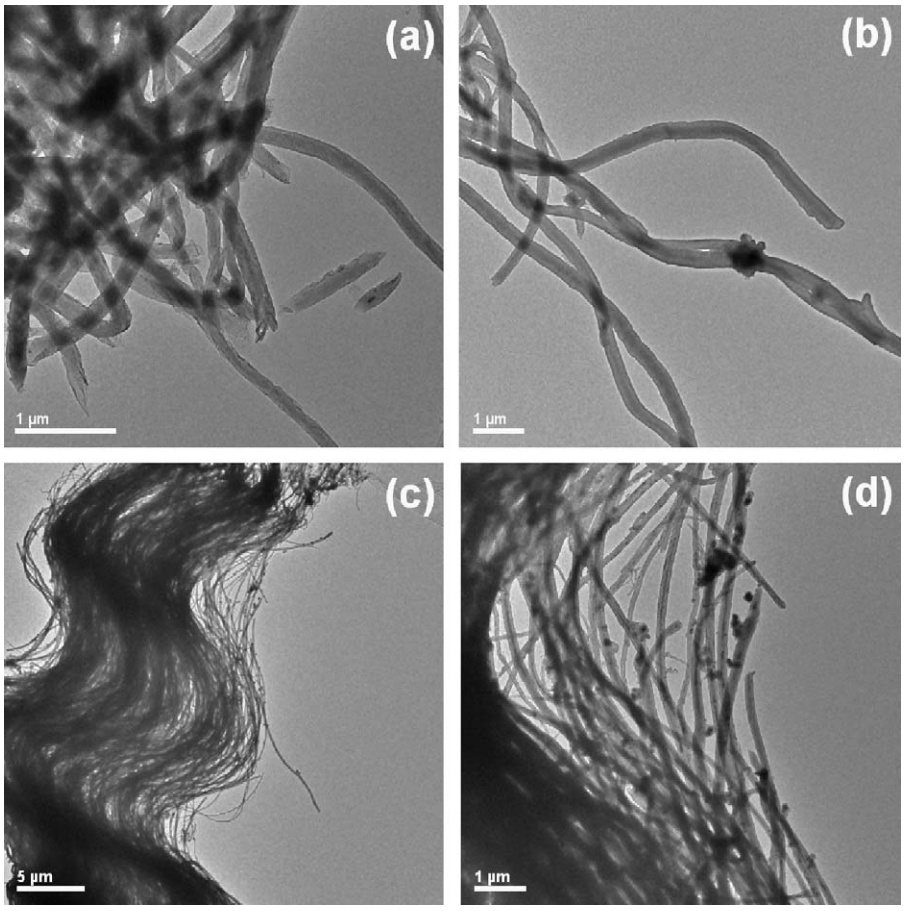

Fig. 7. Transmission electron microscopy images of the carbonaceous samples obtained over the iron oxide film catalyst: (a, b) C/benzene/oxide and (c, d) C/[$Fe_3(CO)_{12}$]/oxide.

4. Conclusions

A novel and simple approach to iron oxide thin film was developed based on a CVD process, starting from ferrocene vapors as precursor and using PVG as substrate. This iron oxide film is a good catalyst to multi-walled carbon nanotubes growth, starting from both pristine benzene and a benzene solution of $[Fe_3(CO)_{12}]$ as precursor. The production of CNTs employing this iron oxide film as catalyst presents some advantages, mainly related to the easiness in the production of the catalyst (previous steps related to the reduction of oxides particles to the preparation of metallic catalysts are not necessary) and the simple apparatus to the CNTs growth.

A very interesting and open question resulting from this work is related to the role of the $[Fe_3(CO)_{12}]$ in the mechanism of CNTs growth. The benzene solution of $[Fe_3(CO)_{12}]$ does not produce CNTs in the absence of the iron oxide film catalyst, probably due to low solubility of $[Fe_3(CO)_{12}]$ in benzene (resulting in a low iron-containing species to catalyze the CNT growth in a similar way as the well-described processes based on ferrocene/benzene solutions). However, the presence of this organometallic compound in the precursor solution makes the obtained CNTs more homogeneous and structurally better when compared with similar samples obtained in the absence of $[Fe_3(CO)_{12}]$. Future efforts will be necessary to clarify this point.

As a final consideration, it is important to note that this route to the iron oxide film deposition can at first be adapted to other kind of substrates (quartz, mica, etc.) and larger areas, which could be important in the large scale production of multi-walled carbon nanotubes.

Acknowledgments

Authors acknowledge the financial support from CNPq, CAPES-PROCAD and Brazilian Network on Carbon Nanotubes Research. We also acknowledge Dr. Marcela Mohallem Oliveira and CME-UFPR for the microscopy images. MCS thanks CAPES for the fellowship.

References

[1] S. Iijima, Nature 354 (1991) 56.
[2] T. Guo, P. Nikolaev, A.G. Rinzler, D. Tomanek, D.T. Colbert, R.E. Smalley, J. Phys. Chem. 99 (1995) 10694.
[3] X.M. Ni, Q.B. Zhao, Y.F. Zhang, H.G. Zheng, Eur. J. Inorg. Chem. 3 (2007) 422.
[4] S. Esconjauregui, C.M. Whelan, K. Maex, Carbon 47 (2009) 659.
[5] M. Terrones, Annu. Rev. Mater. Res. 33 (2003) 419.
[6] M.C. Schnitzler, M.M. Oliveira, D. Ugarte, A.J.G. Zarbin, Chem. Phys. Lett. 381 (2003) 541.
[7] M.C. Schnitzler, A.J.G. Zarbin, J. Nanopart. Res. 10 (2008) 585.
[8] M.C. Schnitzler, A.S. Mangrich, W.A.A. Macedo, J.D. Ardisson, A.J.G. Zarbin, Inorg. Chem. 45 (2006) 10642.
[9] W. Kim, H.C. Choi, M. Shim, Y.M. Li, D.W. Wang, H.J. Dai, Nano Lett. 2 (2002) 703.
[10] M.H. Rummeli, E. Borowiak-Palen, T. Gemming, T. Pichler, M. Knupfer, M. Kalbac, L. Dunsch, O. Jost, S.R.P. Silva, W. Pompe, B. Buchner, Nano Lett. 5 (2005) 1209.
[11] Q. Fu, J. Liu, J. Phys. Chem. B 108 (2004) 6124.
[12] X.J. Dai, C. Skourtis, J. Appl. Phys. 103 (2008) 124305.
[13] D. Barreca, W.J. Blau, G.M. Croke, F.A. Deeney, F.C. Dillon, et al., Microp. Mesop. Mater. 103 (2007) 142.
[14] H. Sato, Y. Hori, K. Hata, K. Seko, H. Nakahara, Y. Saito, J. Appl. Phys. 100 (2006) 104321.
[15] M.J. Massey, U. Baier, R. Merlin, W.H. Weber, Phys. Rev. B 41 (1990) 7822.
[16] Y. Saito, T. Yoshikawa, S. Bandow, H. Tomita, T. Hayashi, Phys. Rev. B 48 (1993) 1907.
[17] H. Kim, W. Sigmund, Carbon 43 (2005) 1743.
[18] F. Tuinstra, J.L. Koenig, J. Chem. Phys. 53 (1970) 1126.
[19] P.C. Eklund, J.M. Holden, R.A. Jishi, Carbon 33 (1995) 959.
[20] A. Cuesta, P. Dhamelincourt, J. Laureyns, A. Martínez-Alonso, J.M.D. Tascón, J. Mater. Chem. 8 (1998) 2875.
[21] M. Sveningsson, R.-E. Morjan, O.A. Nerushev, J. Bäckström, E.E.B. Campbell, F. Rohmund, Appl. Phys. A 73 (2001) 409.